THESIS

FLASH HOLOGRAPHIC MICROSCOPY USING A COMPACT EXTREME ULTRAVIOLET TABLE TOP LASER

Submitted by

Nils C. Monserud

Department of Electrical and Computer Engineering

In partial fulfillment of the requirements

For the Degree of Master of Science

Colorado State University

Fort Collins, Colorado

Spring 2015

Master's Committee:

Advisor: Mario Marconi

Carmon Menoni
Mingzhong Wu

ABSTRACT

FLASH HOLOGRAPHIC MICROSCOPY USING A COMPACT EXTREME ULTRAVIOLET TABLE TOP LASER

Microscopes allow our eyes to visualize objects at micro- and nanoscales. But there application are not limited to static images. The visualization of dynamic processes is necessary to understand complex systems on the micro- and nanoscales, Thus the need for microscopes capable of visualizing nanoscale processes, to further extend the development on micro- and nano-electromechanical devices (MEMS and NEMS). Conventional microscopy will not be sufficient for this purpose for two reasons the first is the spatial resolution is not sufficient to capture nanoscale objects and secondly if the object is moving out of plane the image taken needs to be adjusted using methods of post processing. To this end Fourier transform holography using and EUV light source was utilized to provide us with a method recording sub-micron oscillators.We recorded the oscillation of sub-micron pillars using time resolved extreme ultraviolet (EUV) Fourier transform Holography. The source utilized was a 46.9 nm tabletop capillary discharge with an EUV wavelength of 46.9nm, which provided large flux of coherent illumination. The bright illumination allowed for a modified Fresnel Zone plate to be used as a beam splitter. The modified Fresnel zone plate was able to produce a reference and object beam. This reference and object beam interfered creating a hologram. The reference wave is created by the first order focus while a central opening in the zone plate illuminates the object. Single-shot holograms allowed for the composition of a movie featuring the fast oscillation. Three-dimensional displacements of the object were determined as well by numerical back-propagation, or “refocusing” of the electromagnetic fields during the reconstruction of a single holography.

ACKNOWLEDGEMENTS

I would like to extend my thanks to my mentor Professor Dr. Mario Marconi, and also Dr. Carmen Menoni who have helped me throughout my time at the NSF EUV ERC with all the problems I may have had whether they be big or small. I would also like to thank all of my colleagues who over the years have helped me with my problems along with helpful suggestions around the lab.

I would also like to thank my Family who have supported me throughout this entire endeavor and hope to continue to support me through the rest of my schooling.

TABLE OF CONTENTS

LIST OF FIGURES

1. INTRODUCTION

1.1 MOTIVATION

Recent developments in coherent soft x-ray (SXR) radiation for a wide variety of applications since its demonstration in 1985 [1], [2] have garnered great notoriety. The unique properties of coherent x-ray radiation been the motivation behind the construction of several synchrotron facilities worldwide [3]. But the need for a more compact source of coherent x-ray is evident so the general scientific committee may be able to utilize this powerful laboratory tool. This motivated the development of a few compact SXR and Extreme ultraviolet (EUV) light sources. These light sources span across the SXR and EUV regions as is illustrated Fig. 1-1.

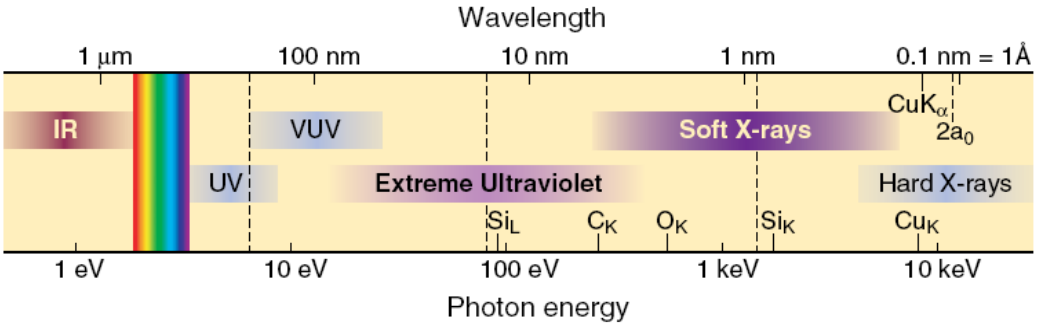

Fig. 1-1: Illustration of the various regions of the electromagnetic spectrum including: infrared (IR), visible, ultraviolet (UV), extreme ultraviolet (EUV), soft X-rays (SXR) and hard X-rays. (from [3])

With the advent of coherent table top light source came imaging tools used for a variety of application. Microscopy has been one of the most convenient application for EUV table top sources. Visible microscopes use visible light and allow the user to observe a large variety of samples under many conditions. Using visible light spatial resolution is limited to $\sim 200\ nm$ [4]. To improve spatial resolution in optical microscopes several techniques have been utilized to gain spatial resolution of $\sim 30\ nm$ but more generally $\sim 100\ nm$. Some of these methods to improve the spatial resolution use non-

conventional approaches such as nonlinear, surface and interference methods as well as the development of confocal fluorescence microscope. A more direct approach to improve spatial resolution is to use shorter wavelengths, such as table top coherent EUV light sources. The spatial resolution of an optical system is proportional to the ratio of the wavelength of illumination over the numerical aperture of the objective, thus by reducing the wavelength a resolution is improved. The lack of short wavelength light sources has limited this approach but due to the light sources discussed above this direct approach can be fully realized.

Over the past decade the fast advance in micro and nano scale technology has drawn great interest throughout the scientific community. The quick advancement in nano-science allowed for several important experimental discoveries in nano-fabrication and in turn a rise in micro-electromechanical systems (MEMS) and nano-electromechanical systems (NEMS). Electromechanical systems have led to the development of NEMS used for ultrasensitive mass detection[1], drug delivery devices[5], and material analysis[6], [7] to list some of the most researched applications in nano-science. In order to develop NEMS and MEMS and to further the understanding of a materials thermal, mechanical and electrical properties is important. Many complex models/theories have been utilized to characterize the behavior of such devices[8], [9]. Experimentally Scanning Electron Microscopes (SEM), Tunneling Electron Microscopes (TEM), and high resolution microscopes have been employed to study materials properties on the nano-scale. Although the TEM and SEM resolution is unparalleled, and capable of imaging objects in the picometer range[10], the spatial and temporal information of the object is lost.

SEM and TEM produce impressive images at magnifications which are on surpassed but they are not cost effective for a small lab to maintain/purchase and the temporal resolution is a must for retrieving the information needed to do many experiments. The theoretical concepts for X-ray holography were first suggested by Baez [11] and Stroke [12]**,** who advocated x-ray wavelengths for use in a high-resolution holographic microscopy. Later Rogers and Plamer [13] postulated the use of zone plates as

beam splitters for use in X-ray holographic microscopy. These theoretical developments led to the initial experiments done by Reuter and Mahr [14] showing it is possible to use X-ray holographic microscopy as a valid means of achieving good resolution at shorter wavelengths although nowhere near the diffraction limit due to several limiting factors such as the available power and the low coherence.

Free electron lasers have been exploited for use in holography[15] due to the degree of spatial and temporal coherence at short wavelengths. It was not until the early 90s when undulator radiation was used to demonstrate high resolution x-ray holography at the national Synchrotron light source and at the Laboratoire d'Utilisation du Rayonne-ment Electromagnetique capable of imaging biological samples with 56 nm resolution [16]. Later I. McNulty and his group using Fourier Transform Holography (FTH) and coherent soft X-ray radiation source provided by the X1A undulator beam line at the National Synchrotron Light source ($\lambda = 3.4\ nm$) McNulty showed the capability of using FTH to image gold sub-micrometer structures. This method was capable of resolving features as small as 60 nm [17].

Fourier transform holography was displayed as a successful technique for single shot imaging with a coherent X-ray free electron source. The source used for this experiment used the high coherent flux, polarization, and photon-energy tenability available at the advanced synchrotron radiation sources at the BESSY-II storage ring with a wavelength of $\lambda = 1.59\ nm$. Similar to the research seen here the dissertation the experiment is setup along the lines of a Fourier transform holography setup with and in plane reference and sample. Here they were capable of resolving images of magnetic nanostructures deposited on to a Si_3N_4 membrane with single pulse from the free electron laser. [18]

The spatial resolution of transmission soft x-ray holographic microscopes using synchrotron radiation has evolved from the micrometer scale resolution down to 15nm resolution all in the past 25 years [19]. Although these experiments have shown holography can be used to obtain the spatial and temporal

data of nano-scale objects, the limited accessibility and the large size of these facilities make them an impractical and inaccessible to the broader scientific community.

The natural progression from using sources at large soft x-ray facilities was to use table top soft x-ray and EUV light sources in Fourier transform holography. High harmonic generation is one of the table top sources used to generate light at ($\lambda = 29\ nm$). the combination of high harmonic generation and Fourier transform holography was able to resolve elbow structures with a resolution of $89\ nm$ under long exposure times of 4800 second exposures. Images were also captured with 30s exposure times to prove a shorter time frame was capable but resolution suffered becoming 125 nm [20]. Table top holography experiments were done in our laboratory by P. Wachulak utilizing capillary discharge lasers and Gabor holography. These precursor experiments were preformed by imaging an Atomic Force Microscope (AFM) cantilever tip using a coherent laser pulse with a wave length of $\lambda = 46.9\ nm$. The images had a spatial resolution of $400\ nm$, [21]

This high resolution was later improved upon buy our group through an experiment again utilizing the EUV capillary discharge laser at $\lambda = 46.9\ nm$ to image a series of carbon nanotubes deposited on a SiN membrane. This time the resolution was found to increase to $46 \pm 2\ nm$ which is approximately the wavelength of illumination, increasing the resolution of the holographic microscope by nearly 8 times [22]. This leads us to another progression in the holographic microscope which will be discussed in this thesis.

This Thesis focusses on a demonstration of Fourier transform holography using a EUV capillary discharge laser at a wavelength of $\lambda = 46.9\ nm$ using Time resolved FTH. The imaging technique utilizes a beam with 1 ns temporal resolution, thus; allowing for the sequential imaging of resonating nano-pillars, oscillating in the MHz frequency range. Chapter 2 provides an introduction and background on the Theory of holography both optical and digital. Chapter 3 describes the experimental procedure along

with the specific tools used in the process of making the holograms. In Chapter 4 the experimental results are shown and discussed along with comparison to models. The conclusion and future directions of the experiment are discussed in Chapter 5.

2. THEORY

2.1. INTRODUCTION- HOLOGRAPHY & DIGITAL HOLOGRAPHY

The goal of holography is not to record a two dimensional intensity pattern but to record the phase as well as the amplitude. To accomplish this a hologram needs two wave fronts (reference and object) in order to generate the interference necessary to be created. This general method may be expanded upon through different three different configurations On-axis holography introduced by Gabor, Off-axis holography introduced by Lieth and Upatnieks, and Fourier holography.

Holography was first introduced by Denis Gabor in 1948 and was proposed to record electron micrographs. Gabor's proof of principle was performed entirely in the optical region. His experiment consists of a two-step process. The first is the recording of the interference pattern between the Fresnel diffraction wave off an object and a reference wave. The second step is the reconstruction of the hologram accomplished through the illumination of the hologram with a reproduction of the reference wave to reproduce your object. This original experiment was done on-axis but the configuration was later modified by Lieth and Upatnieks. Lieth and Upatnieks modified Gabor's experiment to use an off-axis reference. The off-axis reference when reconstructed produced a conjugate images of the original object.

What is focused on here is Fourier holography. Fourier holography is defined as a hologram recorded with the object and the reference in the same plane and parallel (note: the object does not have to be parallel to form a hologram but for objects recorded at a large angles only part of the object may be in focus when reconstructing.) to the holographic recording plane. There is several different configurations of Fourier transform holograms all of which depend on whether they were recorded with or without lenses and the type of illumination (coherent or incoherent). A visible example of a Fourier transform holographic setup may be seen in Fig. 2-1.

2.1.1. FOURIER TRANSFORM

Fourier Transform is a mathematical transformation from the spatial domain to the frequency domain and vice versa. Fourier relationship is valid between two any conjugate magnitudes, not only between spatial and frequency. In its simplest form the Fourier transform in one dimension from the spatial to frequency domain can be defined as

$$\mathcal{F}(f_x) = \int f(x) e^{(j2\pi f_x x)}\, dx$$

With that the inverse Fourier transform defined as

$$f(x) = \int \mathcal{F}(f_x) e^{(j2\pi f_x x)}\, df_x$$

The formalism may be expanded to two dimensions and may be calculated through the two dimensional (spatial) Fourier transform.

$$\mathcal{F}\{g\} = \int \int g(x,y) \mathrm{e}^{[-j2\pi(f_x x + f_y y)]}\, dxdy$$

The transform is a complex value of two independent variables in frequencies f_x and f_y. The inverse Fourier transform may be calculated using

$$\mathcal{F}^{-1}\{G\} = \int \int G(f_x, f_y) \mathrm{e}^{[j2\pi(f_x x + f_y y)]} df_x df_y$$

The two dimensional Fourier transform technique, thus making it ideal for digital image processing which will use a discrete version of a Fourier transform known as a Fast Fourier Transform (FFT) which

will be discussed further in sec. 2.1.3.

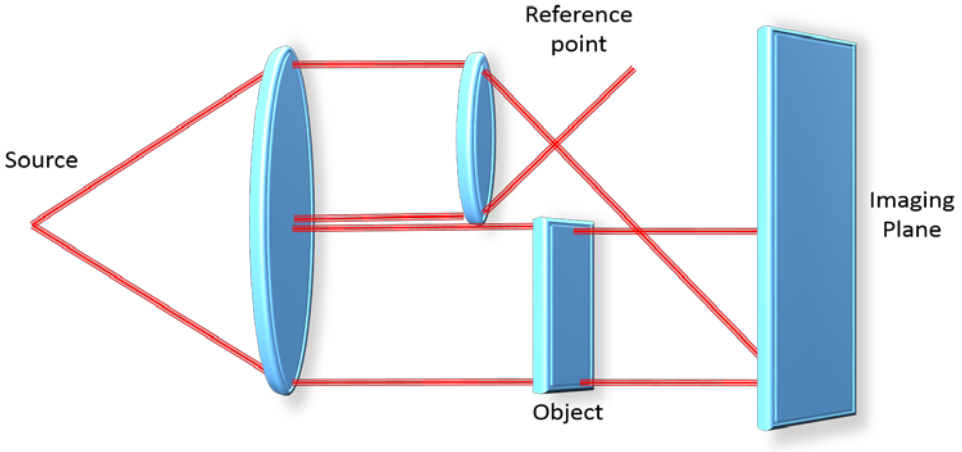

Fig. 2-1: Simple setup for a Fourier transform Holography

2.1.2. HOLOGRAPHY

At visible wavelengths holography has become a highly regarded technique for imaging due to the wide spread use of highly coherent light sources and it's ability to avoid aberrations. With the advent of x-ray sources with high coherence, and high intensity's [23], [24] holographic imaging in the x-ray regime has advanced substantially. Although holography has just begun to gain wide spread use in x-rays especially at the shorter wavelengths (EUV).

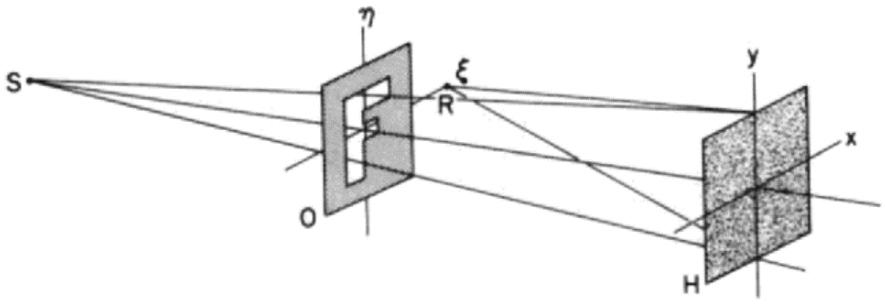

Fig. 2-2: Lensless Fourier-transform hologram

Fig. 2-2 is a pictorial representation of a experimental setup to record a lensless Fourier-transform hologram and will be the type of holography discussed in this paper. In Fourier transform holography

the origin of the reference is a point source simulated by a pinhole and labeled R and produces a point reference source (spherical reference wavefront). Light scatters off the object where upon the light from the object and the spherical reference wave interfere to create the hologram which can then be recorded through use of a photographic film or a charge coupled device (CCD).

2.1.3. DIGITAL HOLOGRAPHY

Holographic microscopy has been seen to be a very sensitive tool for the task of non-destructive testing at high resolutions. Traditional holographic recordings done by Gabor[25] were done on silver halide emulsions/photographic plates thus, the true capability of this method were limited not only by the time scale of the developing process, but also the setup required to view the holograms. These difficulties made it impractical to view recorded holograms at shorter wavelengths. These two factors were solved with the advent of the CCD detector. With the use of a CCD detector the Fourier hologram could be digitally record and reconstruct the holograms produced. This digital reconstruction process is accomplished through the use of a FFT.

When computationally reconstructing a hologram the FFT is an algorithm to compute a discrete Fourier transform. The discrete Fourier transform is the decomposition of a sequence of values into components of different frequencies. The Fourier Transform used here computed an N-point discrete Fourier transform and uses the Cooley-Turkey algorithm. The Cooley-Turkey algorithm is beyond the scope of this paper but more information may be found in the following reference [26].

Digital reconstruction of the image from the hologram gives the user a great degree of freedom to manipulate the waveform form when reconstructing the object. Another advantage is the reconstruction may be preformed in real time thus, allowing for adjustment to your object in real time thus, allowing for the sensing of nano-structures possible.

3. EXPERIMENTAL SETUP

Fig. 3-1: 46.9 nm Ne-like Ar discharge capillary laser and experimental chamber

3.1. INTRODUCTION

Figure 3.1 shows the table top experimental setup of the holographic time resolved system. The EUV laser (right side of Fig. 3-1) is connected to the experiment chamber through a series of vacuum manifolds. The source is a **λ=**46.9 nm Neon (Ne)-like Argon (Ar) discharge-capillary laser. The compact laser main characteristics are: energy per pulse of $\sim 500\ mJ$, a coherence radius of $R_c = 550\ \mu m$ at $15.7\ cm$ from the exit of the capillary and a relative laser spectral bandwidth 3-5 10^{-5} which corresponds to a longitudinal coherence of approximately $L_c = 690\ \mu m$. [27]–[29]

In the experiment chamber is located the holographic setup. Fig. 3-4 is a scheme of the system. The setup is composed of two main components: a 500um diameter, 100nm outermost zone width Fresnel Zone Plate which acts as the beam splitter, and an opaque membrane where the object and the reference are defined.

As was described in Sec. 2.1.2 FTH requires a spherical reference wavefront. For this experiment the illumination and the reference wavefronts are obtained by utilizing a modified FZP acting as a beam splitter. The Scanning Electron Micrograph (SEM) image of the FZP is shown in Fig. 3-2. The scheme depicted in Fig. 3-2 shows a free standing structure fabricated using Electron Beam Lithography tool at Lawarnce Berkeley National Laboratory, using a 100 nm thick Si_3N_4 membrane [30]. In order to

maintain the integrity of the structure of the free standing FZP randomly located bridges hold together the zones is seen in Fig. 3-2 This basic FZP can then be modified into a beam splitter by removing the central region of the structure, effectively leaving an “annular” shaped FZP. The annular shape of the FZP allows for direct illumination of the object down-stream, while the remaining zones focus the laser radiation onto a first order focal point. The modified FZP used in the experiments seen here are a freestanding zone plate with an outer diameter of $D = 500\ \mu m$, a $\Delta r = 100\ \mu m$ central opening, which has 1250 zones. The outer zone width was $100\ nm$ corresponding to a focal distance of $f = 1.07\ mm$ and a numerical aperture of $NA = 0.2345$.

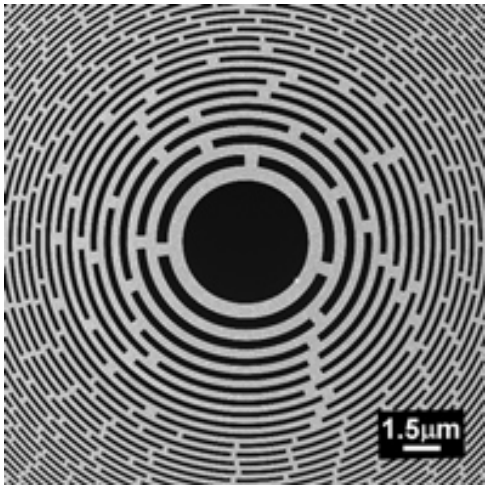

Fig. 3-2: Free Standing Fresnel Zone Plate (FZP) (look for a better image)

According to Sec. 2.1.2 FTH requires an object and a spherical reference wave. The two wavefronts are created by the holographic mask (see sec. 3.4) which is According to Sec. 2.1.2 needs to be coplanar with the object to create the needed spherical reference wave. According to the separation criterion when reconstructing the hologram, the distance from the object to the reference needs to be setup so the image does not overlap with the convolution of itself (see sec. 3.4 for specific numbers). This in turn causes the beam splitter to be set up so the object and the reference are separated by a distance no greater than the radius of the beam splitter central opening therefor allowing both object and reference

to be illuminated while not violating the separation criterion. The Object is made from 200 nm Si_3N_4 membrane coated with 200 nm of gold (Au) using focused ion beam milling (FIB). Two objects were fabricated: the first was a series of 3 pillars $15\ \mu m$ long, $200\ nm$ wide with a period of $500\ nm$. The second object fabricated was a series of pillars $15\ \mu m$ long by $200\ nm$ wide with a period of $2\ \mu m$. The reference pinhole is located $16.7\ \mu m$ from the center of the object and is 500 nm in diameter. A SEM image may be seen in Fig. 3-8. The sample was attached to a piezo electric actuator as shown in Fig. 3-3. The actuator was used to create small movement in the sample in the Y direction (in the plane of the object) too oscillate the pillars at their resonant frequency. The pillars are put into resonances which was found to be anywhere from $0.5 - 2\ MHz$ [31]. The piezo and the object may be seen in Fig. 3-3.

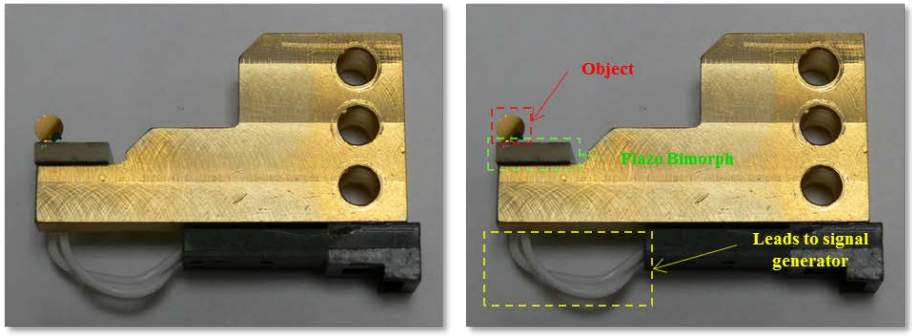

Fig. 3-3: The Piezo Mounted Object without Aluminum Screen

To record the diffraction pattern from the object and the reference wave a CCD detector was used. The diffraction pattern was recorded $5.4\ cm$ from the object with a back illuminated Andor Ikon X-ray CCD detector with $13.5\ \mu m^2$ pixels and a total pixel count of 2048×2048.

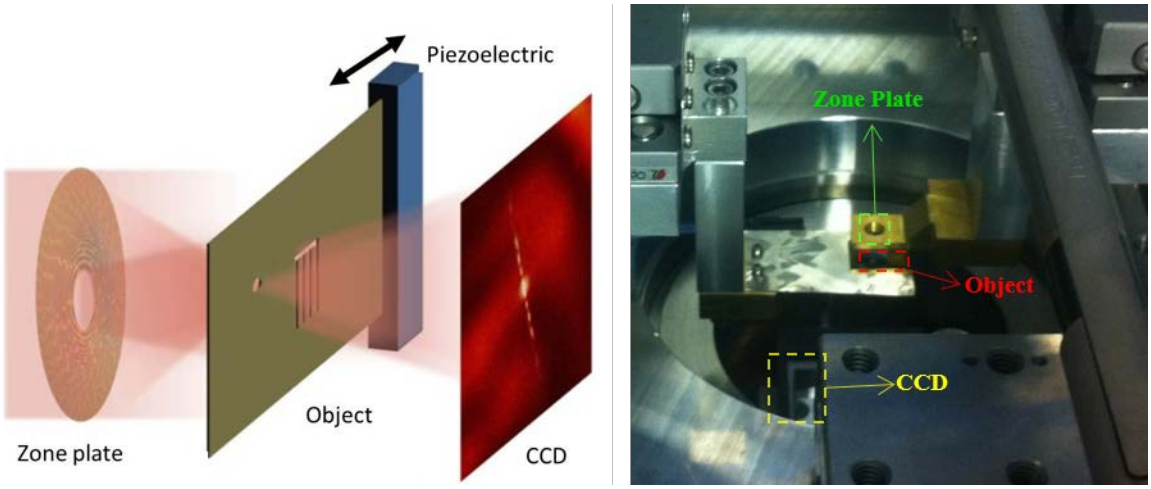

Fig. 3-4: Left, The 46.9 nm beam is incident on a zone plate with central opening. The zone plate allows the first order light to pass through the central opening to illuminate the sample while the higher orders are focused onto a 450 nm pinhole. The light from the sample and the pinhole interfere at the plane of the CCD to produce the pattern which is captured and fed through a Fourier transform to receive the original object. Right, a photo of the actual setup.[34]

3.2. THE EUV TABLE TOP LASER

The laser seen in Fig. 3-1 is a pulsed source. Looking at Fig. 3-5 a large number of atoms will be ionized with electrons promoted to the $1s^2 2s^2 2p^5 3p$ level through electron impact excitation when the plasma column is created. From the upper laser level there is a fast decay and an emission of photons.

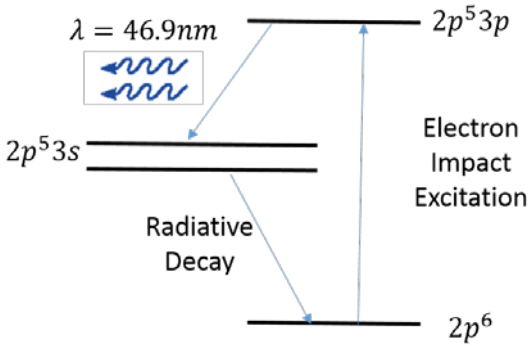

Fig. 3-5: Simplified energy level diagram for Ne-like Ar capillary discharge laser

Holographic imaging at short wavelengths has been the sole domain of synchrotron sources due to the coherence requirements and high average power required at short wavelengths but these facilities are

huge buildings and have limited accessibility[32]. Recently several table top EUV sources have been developed to allow the users to preform holography in a laboratory environment [33]. The capillary discharge lasers are the most powerful table top coherent EUV source available. The laser is capable of emitting a single pulse of $500\ \mu J$. The high photon flux, thus allowing for single shot image acquisition to be performed, which enables the acquisition of time resolved hologram to be recorded as described in this work.

Diffraction limits conventional holography to approximately half the wavelength light used. The spatial resolution can be found through the equation

$$R_{spatial} = \frac{k_1 \lambda}{NA_{ZP}}$$

Where λ is the wavelength of light, k_1 is the coherence of illumination, and NA_{zp} is the numerical aperture of the zone plate. The beam which is emitted from the capillary discharge laser is considered to be fully coherent thus, $k_1 = 1$. If the illumination source is fully coherent there are only two ways to increase resolution increasing the numerical aperture or by decreasing the wavelength which is what is done here the $\lambda = 46.9\ nm$ light used here increases the resolution by a factor of 10, over a conventional hologram using the visible spectrum.

Holography is a coherent imaging technique as discussed in previous chapter and there for will benefit from a highly coherent source. The capillary discharge laser has a high degree of spatial coherence increases with capillary size as seen in Fig. 3-6. In the results discussed here the length of the capillary used was $27\ cm$ which has a high degree of spatial resolution at $R_s = 750\ \mu m$. The laser also has a high degree of temporal (longitudinal) coherence at approximately $L_c = 690\ \mu m$ [27]. Both the high degree of spatial coherence and temporal coherence emitted from the capillary laser are instrumental in obtaining optimal conditions for holographic imaging at wavelengths in and around the EUV spectrum.

Another important consideration is the time scale in order to image an object with a frequency of $0.5 - 2\ MHz$ the pulse length needs to be taken into consideration. For the capillary discharge laser has a 1.2 ns temporal resolution, thus enabling single shot images to be taken of oscillating high frequency pillars.

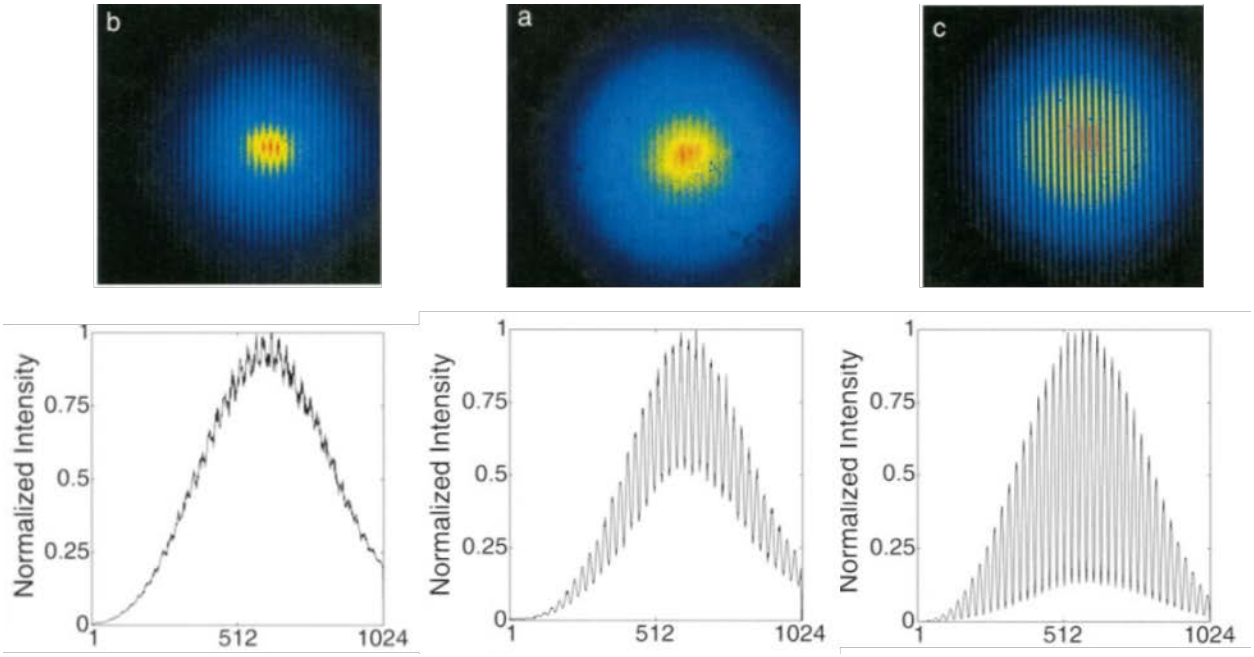

Fig. 3-6: Interferograms and corresponding line outs of capillary's of lengths of 18 cm (a), 27 cm (b), and 37 cm (c). showing an increase in coherence with an increase in capillary length.[28]

3.3. Optics

The advantages to using short wavelengths for holographic imaging have been described in the previous sections but there are some substantial difficulties which makes holographic imaging on short wavelengths difficult.

Because of the laser produces coherent light in the EUV region ($\lambda = 46.9nm$), the beam will have a large absorption coefficient for most materials. This large absorption coefficient for most materials includes air therefor making it necessary to run the experiment in vacuum. If we look at the index of

refraction relating the scattering factors of individual atoms is $n = 1 - \delta + i\beta$ for EUV wavelengths where δ is the refractive index decrement and β is the absorption index. The ratio of $\frac{\beta}{\delta}$ or the ratio of absorption over the refraction index decrement approaches unity for most materials thus, refraction cannot occur within the short absorption length found in most materials. Therefor other methods have to be used in order to manipulate the beam. The use of reflective optics (multilayers mirrors, grazing incidence mirrors) and diffractive optics (zone plates) have to be utilized in order to have enough flexibility to preform experiments in the EUV regime.

3.3.1. REFLECTIVE OPTICS

The two types of reflective optics utilized for work with EUV light are multilayer mirrors and grazing incident mirrors. Grazing incident mirrors will not be discussing because they were not utilized in this experiment. The multilayer mirror used in this experiment was designed to help guide the beam into the experiment chamber while having a high reflectivity or low loss at a wavelength of $\lambda = 46.9nm$. The mirror itself is made up of a series of Scandium (Sc) and Silicon (Si). The two materials maximize the reflectivity of the mirror while minimize the interference effects caused by the light reflecting off the boundary due difference in index. The layers are able to maximize the reflection by having a high Z material (Sc) and a low Z material (Si). The thicknesses of the high Z layers are chosen so the path length differences for reflections from the high index layers are half the wavelength.

3.3.2. DIFFRACTIVE OPTICS

At short wavelengths diffractive optics such as FZP are of great interest due to their ability to provide high spatial resolution near the diffraction limit. In its simplest form a FZP is a circular grating with radial zones increasing in path length enabling the photons to be focused down to a spot on the order of the diffraction limit a pictorial representation may be seen in Fig. 3-7. A FZP is considered a type of lens made through electron beam lithography by making a series of concentric annular zones of alternating

opaque and transmissive material or free space although in the case of a freestanding zone plate there needs to be supports for the zones as may be seen in Fig. 3-2. One disadvantage to working with zone plates is chromatic aberration of zone plates are much larger than that of a typical refractive lens, thus monochromatic illumination needs to be used thus making them ideal for imaging with the coherent light sources such as EUV capillary discharge lasers.

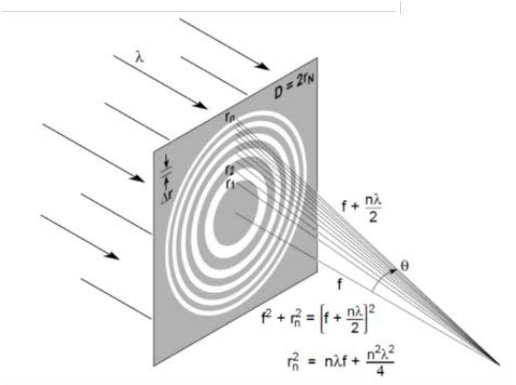

Fig. 3-7: Illustration of diffraction of a Fresnel zone plate[3]

3.4. HOLOGRAPHIC MASK

Fig. 3-8 is a SEM image of the objects used in the experiment. The two objects were fabricated using focused ion beam milling on a 200 nm thick Silicon Nitride (Si_3N_4) membrane with a $200\ nm$ gold (Au) coating. The first object constructed consisted of three pillars $15\ \mu m$ long by $200\ nm$ wide with a period of $200\ nm$ (seen in Fig. 3-8a). The reference pinhole was located $16.7\ \mu m$ away from the sample and

was $500\ nm$ in diameter.

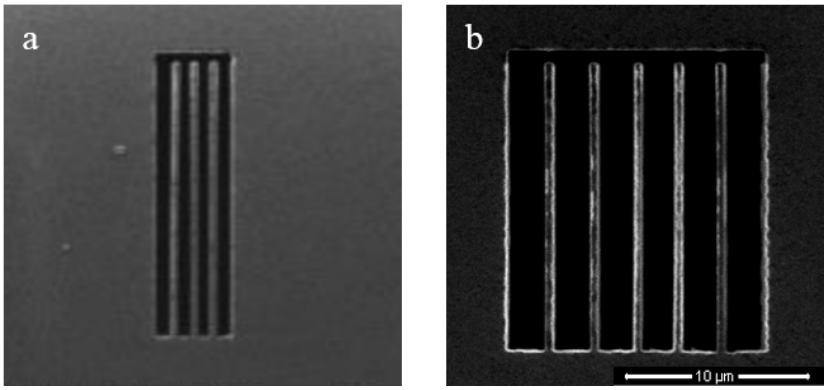

Fig. 3-8: Scanning Electron Microscope (SEM) image of three pillar formation (a) and Five pillar Formation (b) used in

The second object used for the experiment (seen in Fig. 3-8b) consisted of five pillars and is again made of Si_3N_4. The pillars fabricated were $15\ \mu m$ in length by $200\ nm$ wide pillars but with a gap spacing of $2\ \mu m$. The gap spacing was increased compared to the initial sample to adjust for the flexion of the pillars. This sample was also made with a $750\ nm$ reference pinhole and a $500\ nm$ reference pinhole located $30\ \mu m$ away from the sample.

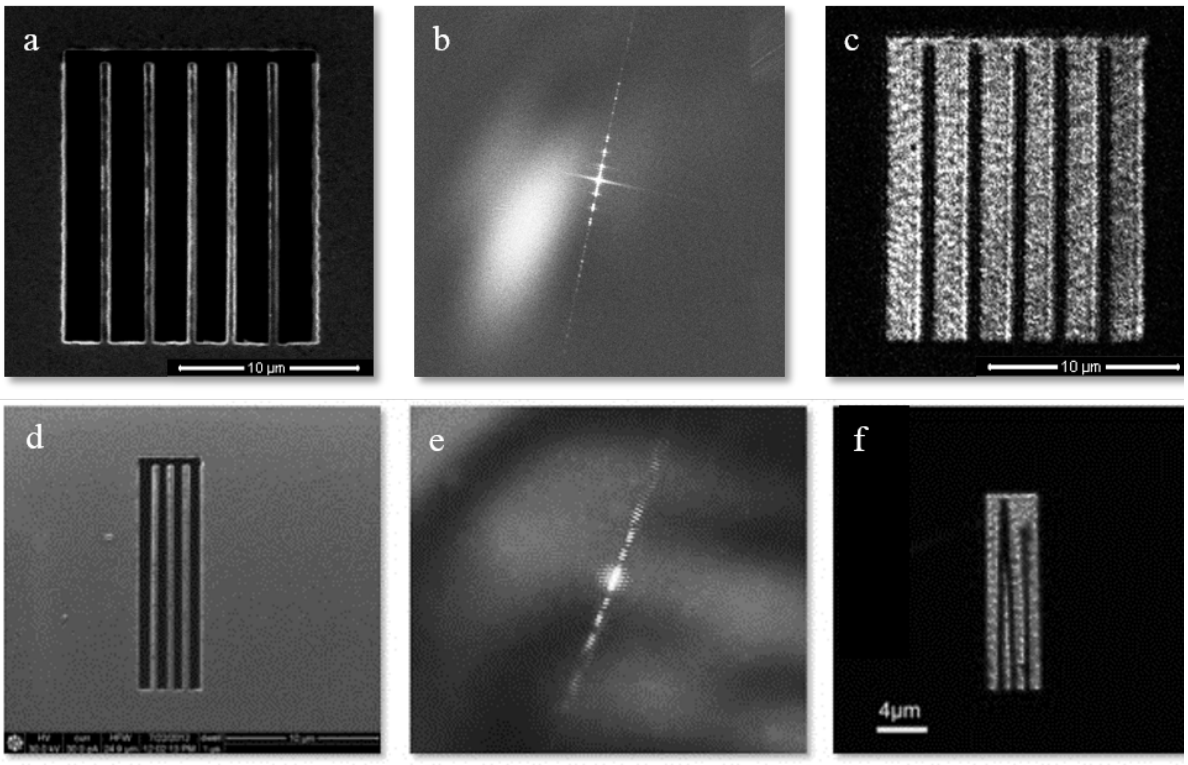

Fig. 4-1, (a) SEM image of three pillar formation. (b) hologram taken with a single shot EUV pulse. (c) Reconstruction of the three pillars from the hologram seen in (b). (d) SEM image of Five pillar Formation (e) hologram taken with a single shot EUV pulse. (f) Reconstruction of the five pillars from the hologram seen in (e).

4.1. RESULTS

Fig. 4-1 seen above is a compilation of images showing the three step process in FLASH imaging, Object, formation of Hologram, and hologram reconstruction. In Fig. 4-1(a,d) an SEM image of the holographic mask is observed in both a three pillar formation (a) and a five pillar formation (b). The Fig. 4-1 (b,c) are the holograms which are formed from the circular reference and the object beam interfering for both the three (b) and five (e) pillar formation. Fig. 4-1 (c,d) is the reconstruction of the three and five pillar hologram. The holographic masks described in detail in sec. 3.4 are set into motion using a piezo electric bimorph. Images of the resonating pillars were captured using flash imaging (1.2 ns exposure time). As described in sec. 3.2 the fast exposure time of the laser allows for “frozen” image of the resonating

nanostructures. The 1.2 ns exposure time is sufficient to record holograms of objects resonating at 1-2Mhz.

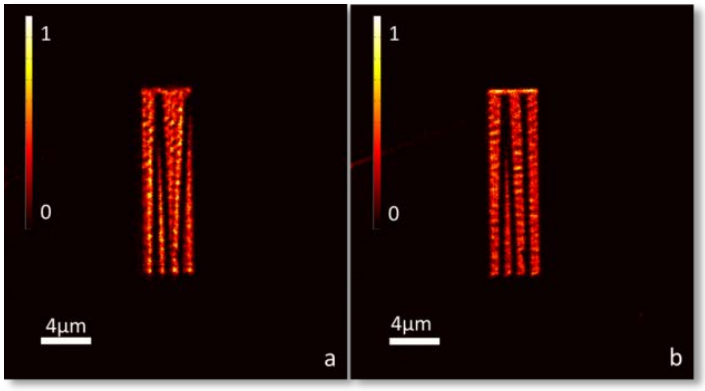

Fig. 4-2 (a-e), Reconstructions of holograms taken using FLASH imaging at different points of beam flection in the dynamic range of the pillar at a freq. of MHz

Fig. 4-2 shows a sequence of reconstructions of the resonating holographic mask acquired at different points in time during the periodic oscillation. As may be seen in the reconstruction of the holograms you clearly see the third pillar from the left is deviating from rest position. Taking single shot holograms consecutively of the resonating pillars one may form a sequence and thus may see the pillars resonating clearly. The motion of the two pillars on the left (stuck together with what is thought to be Van der Walls force) can be seen to resonate in unison using this technique.

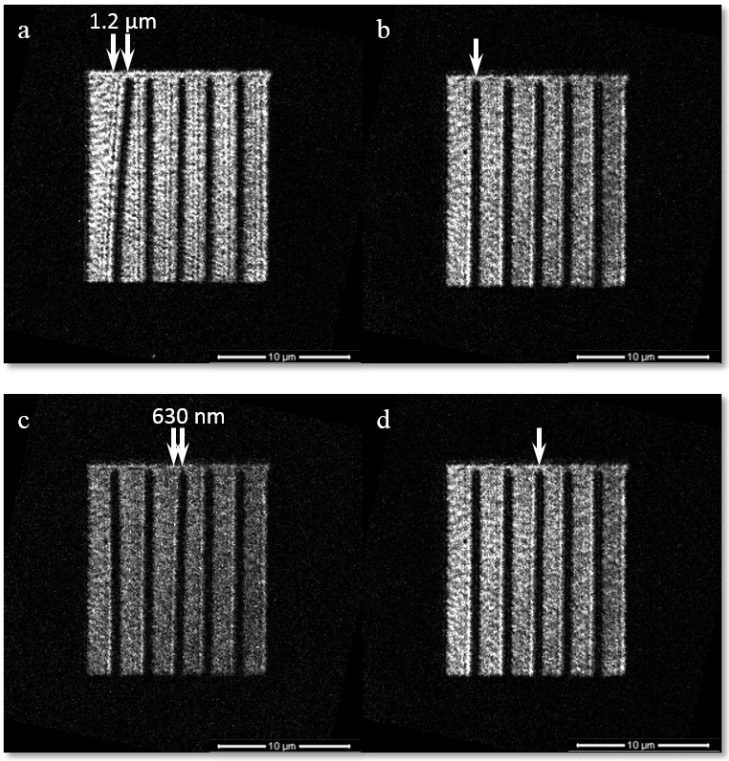

Fig. 4-3, Reconstructions of holograms taken using FLASH imaging. (a,b) the pillars are driven at a freq of 487.5 KHz with a tip deviation $\sim 1.2\ \mu m$. (c,d) the pillars are driven at a freq of 489.0 KHz with a tip deviation$\sim .630\ nm$.

Fig. 4-3 is a reconstruction of four holograms taken at two different excitation frequencies demonstrating the pillars may be excited individually due to the small differences in size. In Fig. 4-3 (a,b) the piezo actuator is excited with a sinusoidal signal of $487.5\ kHz$, when excited at this frequance it was observed the only pillar set into motion was the first from the left. Due to the variability in fabrication of the pillars the five pillars seen in Fig. 4-3 are not identical in all dimensions. Due to the variability in dimensions it was expected that each pillar would have its own resonant frequency. This variation in frequency change due to variations in the pillars may be observed in the change in holograms in Fig. 4-3. In the (a,b) holograms to the (c,d) holograms the change frequency was from $487.5\ KHz$ to $489\ KHz$ this change may be visually observed when the first pillar stops resonating and the third pillar from the

left begins to resonate. From the visual analysis the pillars resonating at $487.5\ KHz$ had a tip deviation of $\sim 1.2\ \mu m$ while the pillars resonating at $489.0\ KHz$ had a tip deviation of $\sim 0.63\ \mu m$. [34]

The flash imaging presented in this work enables the evaluation of the oscillating dynamics of nanoscale oscillator. Through the detection of different resonant frequencies in the array it is possible to correlate differences in size. The information obtained from the images may be used to benchmark the model of oscillating pillars that we demonstrated and can be considered as a first order Euler's cantilevers.

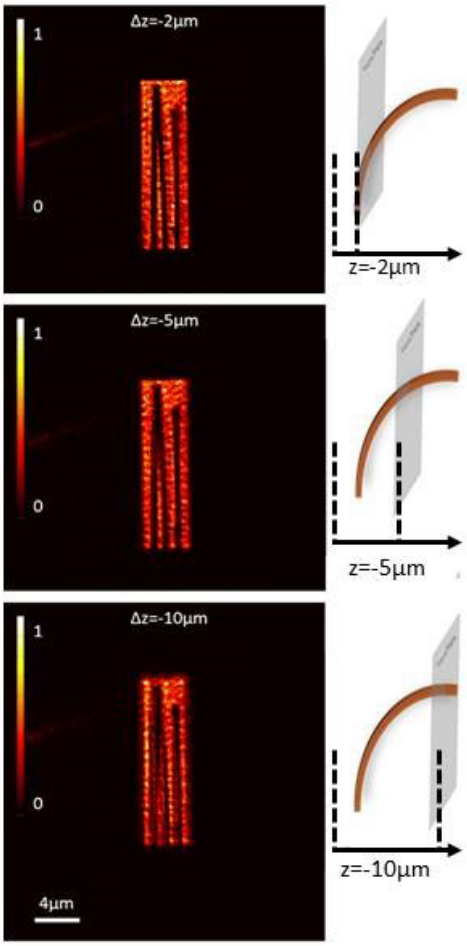

Fig. 4-4, The left column is the three reconstruction at three different depths (z=$-2, -5, and -10\ \mu m$) using a single shot hologram. (a) The bottom section appears in focus $z = -2\ \mu m$, (b) the center section aperas in focus at $z = -5\ \mu m$, and (c) the top section appears in focus at $z = -10\ \mu m$. The column to the right shows the plane where the image was reconstructed in relation to the pillar bend.[31]

Additionally the information in the hologram allows for numerical refocusing of the object utilizing Fresnel back-propagation and studying the images at different depths to determine at what depth the image is in focus. Fig. 4-4 shows three reconstructions at different planes in the z direction (along the optical axis) from the image seen in Fig. 4-1 (f). The reconstruction depths were at three different points in the z-axis Fig. 4-4(a) $z = -2\ \mu m$, Fig. 4-4 (b) $z = -5\ \mu m$ and Fig. 4-4 (c) $z = -10\ \mu m$. By using the schematic in the left column of Fig. 4-4 you may see a good representation of what plane the hologram is in focus. This 3D profile of the image allows for precise representation when modeling and determining the position of the tips in time resolved dynamics. Along the optical axis the resolution is limited to the Depth Of Focus (DOF) of the zone plate which in the experiment discussed here is $DOF \cong \pm 430\ nm$. Thus allowing the out of plane analysis to determine the deflection of the right most pillar in Fig. 4-4 to be $\Delta z = 8 \pm 0.43\ \mu m$ relative to the bottom of the pillar.

4.2. DISCUSSION

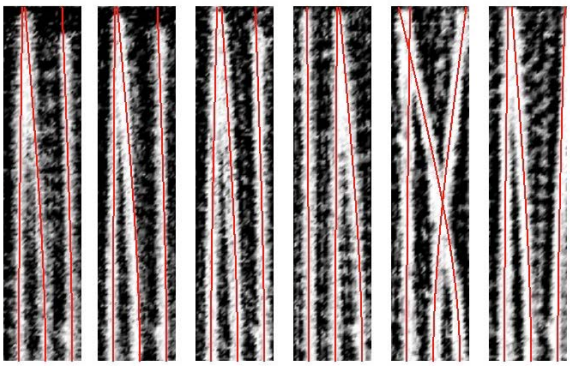

Fig. 4-5 Example of analysis of holograms to Euler's beam/cantilevers. Redlines are the best fits corresponding to vibrating cantilever.[31]

During these experiments we were able to map every aspect of the object (both time scale and size.) The pillar shape can be described with high accuracy no matter the direction of resonation, thus the pillar shape and movement can be described by the first Euler beam resonant shape. Any three

dimensional pillar shape observed in the experiment can be approximated to a high accuracy by a single two dimensional vector describing the components of amplitude of deflection in the directions transverse and parallel to the axis. This is the type of data needed for a direct comparison to the two dimensional model developed in [35], [36]. It was shown under the right conditions, the system captured is highly nonlinear, localized, periodic states known as Intrinsic Localized Modes (ILMs). Fig. 4-5 is in good agreement with the model and validates that a two dimensional vector model can describe the nonlinear theory of interacting pillar arrays [37].

5. SUMMARY & FUTURE WORK

In summary single-shot EUV Fourier transform holography was implemented for the purpose of determining the dynamics of fast moving nanoscale objects in the 0-2 MHz range, which in this case are a series of three and a series of five oscillating pillars. FLASH imaging technique was made possible through the short $1.2\ ns$ duration of the capillary discharge laser illumination. The ability to reconstruct and refocus the object from the hologram allowed for three dimensional pillar displacement characterization.

The present work is to develop a process to print pillars on the scales needed in order to build the samples on site. Future work and considerations will be to observe real-time motion of ILMs on the nanoscale. The next step after that is to use these ILMs to detect foreign objects which may alter pillar dynamics again on the nanoscale seen in this work

6. REFERENCES

[1] S. Suckewer, C. Skinner, and H. Milchberg, “Amplification of stimulated soft x-ray emission in a confined plasma column,” *Phys. Rev. …*, vol. 55, no. 17, 1985.

[2] D. Matthews, P. Hagelstein, and M. Rosen, “Demonstration of a soft x-ray amplifier,” *Phys. Rev. …*, vol. 54, no. 2, 1985.

[3] D. Attwood, *Soft X-Rays and Extreme Ultraviolet Radiation: Principles and Applications*. Cambridge University Press, 2007, p. 470.

[4] Y. Garini, B. J. Vermolen, and I. T. Young, “From micro to nano: recent advances in high-resolution microscopy.,” *Curr. Opin. Biotechnol.*, vol. 16, no. 1, pp. 3–12, Feb. 2005.

[5] M. Staples, K. Daniel, M. J. Cima, and R. Langer, “Application of micro- and nano-electromechanical devices to drug delivery.,” *Pharm. Res.*, vol. 23, no. 5, pp. 847–63, May 2006.

[6] C.-Y. Nam, P. Jaroenapibal, D. Tham, D. E. Luzzi, S. Evoy, and J. E. Fischer, “Diameter-dependent electromechanical properties of GaN nanowires.,” *Nano Lett.*, vol. 6, no. 2, pp. 153–8, Feb. 2006.

[7] V. Cimalla, J. Pezoldt, and O. Ambacher, “Group III nitride and SiC based MEMS and NEMS: materials properties, technology and applications,” *J. Phys. D. Appl. Phys.*, vol. 40, no. 20, pp. 6386–6434, Oct. 2007.

[8] B. H. Houston, D. M. Photiadis, M. H. Marcus, J. a. Bucaro, X. Liu, and J. F. Vignola, “Thermoelastic loss in microscale oscillators,” *Appl. Phys. Lett.*, vol. 80, no. 7, p. 1300, 2002.

[9] P. Lu, H. P. Lee, C. Lu, and P. Q. Zhang, “Dynamic properties of flexural beams using a nonlocal elasticity model,” *J. Appl. Phys.*, vol. 99, no. 7, p. 073510, 2006.

[10] R. Erni, M. Rossell, C. Kisielowski, and U. Dahmen, “Atomic-Resolution Imaging with a Sub-50-pm Electron Probe,” *Phys. Rev. Lett.*, vol. 102, no. 9, p. 096101, Mar. 2009.

[11] A. Baez, “A study in diffraction microscopy with special reference to X-rays,” *JOSA*, vol. 42, no. 10, pp. 756–762, 1952.

[12] G. Stroke and R. R. III, “Holography with spatially noncoherent light,” *Appl. Phys. Lett.*, vol. 7, no. 9, pp. 229–231, 1965.

[13] G. L. Rogers and J. Palmer, “The possibilities of X-ray holographic microscopy*,” *J. Microsc.*, vol. 89, no. 1, pp. 125–135, Feb. 1969.

[14] B. Reuter and H. Mahr, “Experiments with Fourier transform holograms using 4.48 nm X-rays,” *J. Phys. E.*, vol. 9, no. 9, pp. 746–751, Sep. 1976.

[15] H. N. Chapman, S. P. Hau-Riege, M. J. Bogan, S. Bajt, A. Barty, S. Boutet, S. Marchesini, M. Frank, B. W. Woods, W. H. Benner, R. a London, U. Rohner, A. Szöke, E. Spiller, T. Möller, C. Bostedt, D. a Shapiro, M. Kuhlmann, R. Treusch, E. Plönjes, F. Burmeister, M. Bergh, C.

Caleman, G. Huldt, M. M. Seibert, and J. Hajdu, “Femtosecond time-delay X-ray holography.,” *Nature*, vol. 448, no. 7154, pp. 676–9, Aug. 2007.

[16] S. Shu and M. Sharnoff, “Coherent Radiation for X-Ray Imaging-The Soft X-Ray Undulator and the XlA Beamline at the NSLS,” *J. x-ray Sci. technoolgy*, vol. 2, pp. 274–296, 1990.

[17] I. McNulty, J. Kirz, and C. Jacobsen, “High-resolution imaging by Fourier transform X-ray holography,” *Science (80-.).*, vol. 256, no. 5059, pp. 1009–1012, 1992.

[18] S. Elsebitt, “Lensless imaging of magnetic nanostructures by X-ray,” *Lett. to Nat.*, vol. 432, no. December, pp. 885–888, 2004.

[19] W. Chao, B. D. Harteneck, J. A. Liddle, E. H. Anderson, and D. T. Attwood, “Soft X-ray microscopy at a spatial resolution better than 15 nm.,” *Nature*, vol. 435, no. 7046, pp. 1210–3, Jun. 2005.

[20] R. L. Sandberg, D. a. Raymondson, C. La-o-vorakiat, a. Paul, K. S. Raines, J. Miao, M. M. Murnane, H. C. Kapteyn, and W. F. Schlotter, “Tabletop soft-x-ray Fourier transform holography with 50 nm resolution,” *Opt. Lett.*, vol. 34, no. 11, p. 1618, May 2009.

[21] P. W. Wachulak, R. a. Bartels, M. C. Marconi, C. S. Menoni, J. J. Rocca, Y. Lu, and B. Parkinson, “Sub 400 nm spatial resolution extreme ultraviolet holography with a table top laser,” *Opt. Express*, vol. 14, no. 21, p. 9636, 2006.

[22] P. W. Wachulak, M. C. Marconi, R. a. Bartels, C. S. Menoni, and J. J. Rocca, “Soft x-ray laser holography with wavelength resolution,” *J. Opt. Soc. Am. B*, vol. 25, no. 11, p. 1811, Oct. 2008.

[23] J. J. Rocca, O. D. Cortzar, B. Szapiro, K. Floyd, and F. G. Tomasel, “Fast-discharge excitation of hot capillary plasmas for soft-x-ray amplifiers,” *Physical Review E*, vol. 47, no. 2. pp. 1299–1304, 1993.

[24] M. Tegze and G. Faigel, “X-ray holography with atomic resolution,” *Nature*, vol. 380, no. 6569, pp. 49–51, Mar. 1996.

[25] D. Gabor, “Microscopy by reconstructed wave-fronts.,” *Proc. Phys. Soc.*, vol. 64, no. 374 B, pp. 449–469, Sep. 1951.

[26] J. W. and J. W. T. Cooley, “An Algorithm for the Machine Computation of the Complex Fourier Series_Cooley.pdf,” *Math. Comput.*, vol. 19, no. 90, pp. 297–301, 1965.

[27] L. Urbanski, M. C. Marconi, L. M. Meng, M. Berrill, O. Guilbaud, a. Klisnick, and J. J. Rocca, “Spectral linewidth of a Ne-like Ar capillary discharge soft-x-ray laser and its dependence on amplification beyond gain saturation,” *Phys. Rev. A*, vol. 85, no. 3, p. 033837, Mar. 2012.

[28] Y. Liu, M. Seminario, F. G. Tomasel, C. Chang, J. J. Rocca, and D. T. Attwood, “Achievement of essentially full spatial coherence in a high-average-power soft-x-ray laser,” *Phys. Rev. A - At. Mol. Opt. Phys.*, vol. 63, no. 3, pp. 1–5, Feb. 2001.

[29] B. R. Benware, C. D. Macchietto, C. H. Moreno, and J. J. Rocca, “Demonstration of a High Average Power Tabletop Soft X-Ray Laser,” *Phys. Rev. Lett.*, vol. 81, no. 26, pp. 5804–5807, 1998.

[30] E. H. Anderson, “Specialized Electron Beam Nanolithography for EUV and X-Ray Diffractive Optics,” *IEEE J. Quantum Electron.*, vol. 42, no. 1, pp. 27–35, Jan. 2006.

[31] N. C. Monserud, E. B. Malm, P. W. Wachulak, V. Putkaradze, G. Balakrishnan, W. Chao, E. Anderson, D. Carlton, and C. Mario, “Recording oscillations of sub-micron size cantilevers by extreme ultraviolet Fourier transform holography,” *Opt. Express*, vol. 22, no. 4, pp. 4161–4167, 2014.

[32] a. Snigirev, I. Snigireva, V. Kohn, S. Kuznetsov, and I. Schelokov, “On the possibilities of x-ray phase contrast microimaging by coherent high-energy synchrotron radiation,” *Rev. Sci. Instrum.*, vol. 66, no. 12, p. 5486, 1995.

[33] R. Sandberg, A. Paul, D. Raymondson, S. Hädrich, D. Gaudiosi, J. Holtsnider, R. Tobey, O. Cohen, M. Murnane, H. Kapteyn, C. Song, J. Miao, Y. Liu, and F. Salmassi, “Lensless Diffractive Imaging Using Tabletop Coherent High-Harmonic Soft-X-Ray Beams,” *Phys. Rev. Lett.*, vol. 99, no. 9, p. 098103, Aug. 2007.

[34] N. C. Monserud, E. B. Malm, P. W. Walchulk, H. Xu, G. Balakrishnan, W. Chao, E. Anderson, and M. C. Marconi, “Flash extreme ultraviolet holographic microscopy in a table top setup,” *Three-Dimensional Multidimens. Microsc. Image Acquis. Process. XXI, Thomas G. Brown; Carol J. Cogswell; Tony Wilson, Ed. Proc. SPIE Vol. 8949 (SPIE, Bellingham, WA 2014), 89490K.*, vol. 8949, no. Ccd, pp. 1–4, 2014.

[35] D. Brake and V. Putkaradze, “Simplified models for Intrinsic Localized Mode dynamics,” *Proc. 2012 Int. …*, 2012.

[36] D. Brake, H. Xu, A. Hollowell, G. Balakrishnan, C. Hains, M. Marconi, and V. Putkaradze, “Intrinsic localized modes in two-dimensional vibrations of crystalline pillars and their application for sensing,” *J. Appl. Phys.*, vol. 112, no. 10, p. 104326, 2012.

[37] A. J. Sievers, “Intrinsic Localized Modes in Anharmonic,” *Physcical Rev. Lett.*, vol. 61, no. 8, pp. 970–973, 1988.